Synthesis and Luminescence Properties of Two-Electron Bimetallic Cu-Ag and Cu-Au Nanoclusters via Copper Hydride Precursors

Rhone P. Brocha Silalahi, Tzu-Hao Chiu, Jhen-Heng Kao, Chun-Yen Wu, Chi-Wei Yin, Yu-Chiao Liu, Yuan Jang Chen, Jean-Yves Saillard, Ming-Hsi Chiang, C. W. Liu

Synthesis and Luminescence Properties of Two-Electron Bimetallic Cu-Ag and Cu-Au Nanoclusters Via Copper Hydride Precursors

Rhone P. Brocha Silalahi,[§] Tzu-Hao Chiu,[§] Jhen-Heng Kao,[§] Chun-Yen Wu,[§] Chi-Wei Yin,[†] Yu-Chiao Liu,[¥] Yuan Jang Chen,[†]* Jean-Yves Saillard,[£] Ming-Hsi Chiang,[¥]* and C. W. Liu[§]*

[§]Department of Chemistry, National Dong Hwa University No. 1, Sec. 2, Da Hsueh Rd. Shoufeng, Hualien, Taiwan 974301 (R.O.C.) E-mail:chenwei@mail.ndhu.edu.tw

[†]Department of Chemistry, Fu Jen Catholic University 510 Zhongzheng Rd, Xinzhung Dist. New Taipei City, Taiwan 24205 (R.O.C.)

[¥]Institute of Chemistry, Academica Sinica, Taipei, Taiwan, 11528 (R.O.C.)

[£] Univ Rennes, CNRS, ISCR-UMR 6226, Rennes F-35000, France

Keywords: superatom, bimetallic, luminescence, copper, silver, gold

ABSTRACT: The synthesis, structural characteristics, and photophysical properties of luminescent Cu-rich bimetallic superatomic clusters $[Au@Cu_{12}(S_2CN^nPr_2)_6(C{\equiv}CPh)_4]^+$ (**1a**$^+$), $[Au@Cu_{12}\{S_2P(OR)_2\}_6(C{\equiv}CPh)_4]^+$ (**2**$^+$**),** (**2a**$^+$ = ^{i}Pr; **2b**$^+$ = ^{n}Pr), $[Au@Cu_{12}\{S_2P(C_2H_4Ph)_2\}_6(C{\equiv}CPh)_4]^+$ (**2c**$^+$), and $[Ag@Cu_{12}\{S_2P(O^nPr)_2\}_6(C{\equiv}CPh)_4]^+$ (**3**$^+$) were studied. Compositionally uniform clusters **1**$^+$**-3**$^+$ were isolated from the reaction of dithiolato-stabilized, polyhydrido copper clusters with phenylacetylene in the presence of heterometal salts. By using X-ray diffraction, the structures of **1a**$^+$, **2a**$^+$, **2b**$^+$, and **3**$^+$ were able to be determined. ESI-mass spectrometry and elemental analysis confirmed their compositions and purity. The structural characteristics of these clusters are similar to display gold (or silver)-centered Cu_{12} cuboctahedra surrounded by six dithiocarbamate/dithiophosph(in)ate and four alkynyl ligands. The doping of Au and Ag atoms into the polyhydrido copper nanoclusters significantly enhances their PL quantum yields from $Ag@Cu_{12}$ (0.58%) to $Au@Cu_{12}$ (55%) at ambient temperature in solution. In addition, the electrochemical properties of the new alloys were investigated by cyclic voltammetry.

Introduction

Bimetallic nanoclusters (NCs) are extensively studied because of their ability to tune the various properties (optical, catalytic, etc.) and possibly improve the stability of their monometallic counterparts in a controlled way.[1,2] Photoluminescence (PL) is one of the major properties broadly explored in bimetallic NCs,[3] owing to its potential applications in bioimaging, cell labeling, chemical sensing, drug delivery, or phototherapy.[4] The PL of NCs can be tuned by several methods, such as aggregation-induced emission,[5] cluster-based networks via self-assembly of the NC building blocks,[6] alloying metal kernels,[7] and engineering peripheral ligands.[8] However, bimetallic copper-based clusters with a high PL quantum yield (QY) are still rarely reported. Notable examples are $Au_2Cu_6(PPh_2Py)_2(SC_{10}H_{15})_6$ (QY=11.7%), [5a,8a] $[Au_7Cu_{12}(dppy)_6(TBBT)_6Br_4](SbF_6)_3$ (QY=13.2%), [9] and $[AuCu_{14}(SPh^tBu)_{12}(PPh(C_2H_4CN)_2)_6]^+$ (QY=71.3%).[10] Hence, new synthetic methodologies for the isolation of copper alloy NCs with excellent quantum efficiency are still needed. In this research, we report new bimetallic two-electron NCs based on copper that can be synthesized by both alloying the metal kernel and engineering the peripheral ligands to exhibit a high QY of 55%.

In previous studies, a series of copper-rich bimetallic 2-electron NCs, $[M@Cu_{12}(S_2CN^nBu_2)_6(C\equiv CPh)_4]^+$ (M = Au, Ag), were obtained by a galvanic exchange strategy involving the reaction of $[Cu_{13}(S_2CN^nBu_2)_6(alkynyl)_4]^+$ as a template with M(I) salts.[11] The doped species show differences in their optical and electronic properties and stability compared to their template precursor. In particular, the Au-doped cluster exhibits a high PL intensity with QY=59% at 77 K in MeTHF.[11] Later, we uncovered that similar bimetallic Cu-rich NCs stabilized by 1,1-dithiophosphate ligands can shift both emission and absorption spectra to higher energy and display high QY at ambient temperature.

Herein, we report the synthesis of Cu-Au and Cu-Ag clusters generated from the treatment of excess amounts of phenylacetylene with dithiolato-stabilized copper hydrides in the presence of Au(I) and Ag(I) salts. This methodology is totally different from our previously reported procedure of templated galvanic replacement.[11] These clusters have a centered-cuboctahedral $M@Cu_{12}$ kernel surrounded by six dithiocarbamate/dithiophosph(in)ate and four alkynyl ligands with one counteranion to balance the cluster charge. These cationic NCs show idealized T_d symmetry and possess two free n_s valence electrons (n_s = 13-6-4-1), making them pseudospherical 2-electron superatoms with a $1S^2$ configuration.[12] Varying both the nature of M

(Ag, Au) and of the dithiolate ligands allows the tuning of the stability, optical and PL properties of the considered NCs, as described below.

Results and Discussion

Synthesis and Characterization

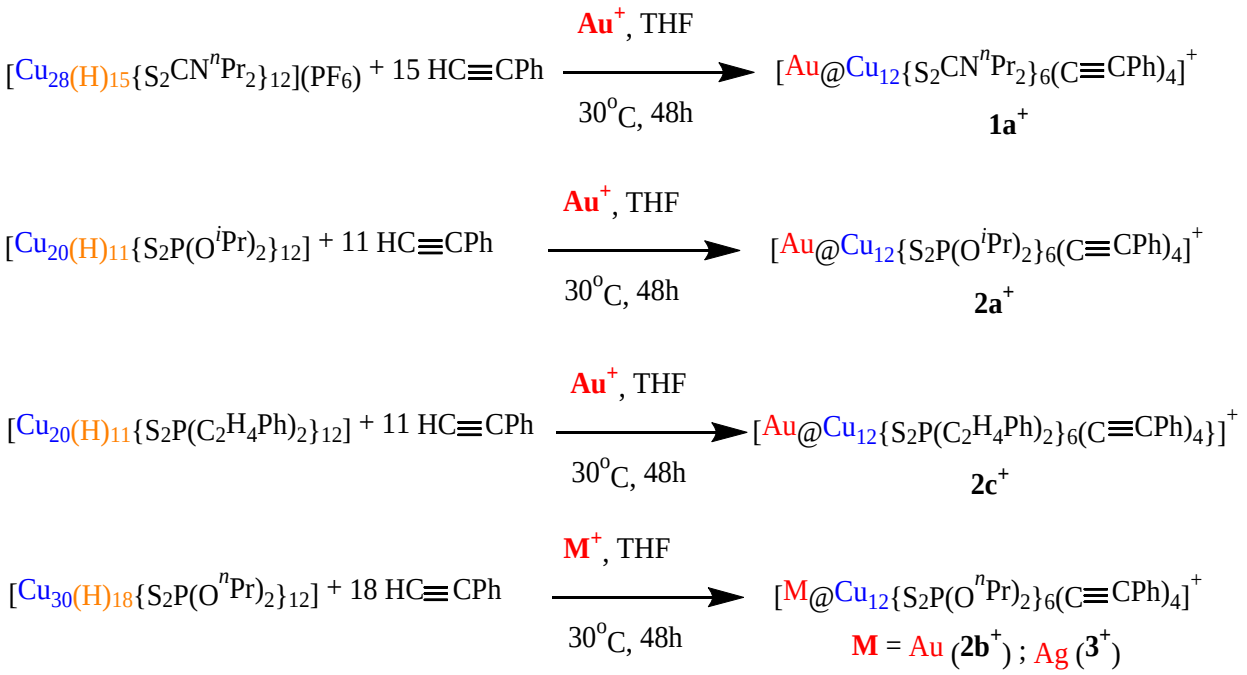

Scheme 1. Synthesis of **1a**$^+$, **2a**$^+$, **2b**$^+$, **2c**$^+$ and **3**$^+$.

We previously reported the synthesis of 2-electron M@Cu_{12} (M = Ag, Au) clusters obtained from a galvanic replacement reaction using $[Cu_{13}\{S_2CN^nBu_2\}_6(C{\equiv}CPh)_4]^+$ as a template.[11] In this paper, we describe a new synthetic procedure from as-synthesized copper(I) hydrides with terminal alkynes in the presence of Au(I) or Ag(I) salts (Scheme 1). This approach allows the use of either dithiocarbamate or dithiophosph(in)ate as stabilizing ligands.

An equimolar amount of $Au(PPh_3)Cl$ was added to a THF suspension of $[Cu_{28}H_{15}\{S_2CN^nPr_2\}_{12}](PF_6)$,[13] followed by the addition of fifteen equiv. of phenylacetylene. The mixture was stirred for 48 hours at 30°C. Purifications led to the generation of the $(CuCl_2)^-$ salt of $[AuCu_{12}\{S_2CN^nPr_2\}_6(C{\equiv}CPh)_4]$ (**1a**$^+$) as a dark red solid in 39% yield (Scheme 1). In this reaction, $[Cu_8H(S_2CN^nPr_2)_6]^+$ was isolated as a byproduct. The positive-ion ESI mass spectrum of **1a**$^+$ clearly shows a prominent band at m/z 2420.60 (calcd 2420.30) corresponding to the molecular ion [**1a**$^+$], and its simulated and experimental isotopic patterns are in perfect

agreement (Figure S1). In the negative-ion ESI mass spectrum, a band at m/z 134.9 (calcd 134.8) can be assigned to the $(CuCl_2)^-$ counteranion (Figures S2). The latter species was obviously formed via the liberation of free Cu(I) in the presence of free chlorides from $Au(PPh_3)Cl$. The ^1H and ^{13}C NMR spectra of **1a**$^+$ show one type of ligand signal for both alkyl dithiocarbamate and alkynyl ligands, suggesting that **1a**$^+$ is highly symmetric in solution (Figure S3-S4). The FT-IR spectra revealed the $\nu(PhC{\equiv}C^-)$ stretching frequency at 2018.7 cm^{-1}, (Figure S5) which is lower than that of free phenylacetylene (ν = 2110 cm^{-1}) and comparable with those in $[Au@Cu_{12}\{S_2CN^nBu_2\}_6(C{\equiv}CPh)_4]^+$ (**1b**$^+$) (2015 cm^{-1}).[11]

Compounds **2a**$(CuCl_2)$ and **2b**(Cl) were synthesized by reacting copper(I) hydrides, $[Cu_{20}H_{11}\{S_2P(O^iPr)_2\}_9]$[14] and $[Cu_{30}H_{18}\{S_2P(O^nPr)_2\}_9]$,[15] respectively, with one equivalent of $Au(PPh_3)Cl$ in the presence of eleven (**2a**$^+$) and eighteen (**2b**$^+$) equiv. of phenylacetylene at 30°C. Immediate workup of the mixture led to the isolation of $[AuCu_{12}\{S_2P(OR)_2\}_6(C{\equiv}CPh)_4]^+$, where R = ^{i}Pr (**2a**$^+$, 44% yield) and ^{n}Pr (**2b**$^+$, 42% yield) as red precipitates. By a synthetic method similar to **2a**$^+$, the $(CuCl_2)^-$ salt of **2c**$^+$ was also isolated as a red precipitate (49% yield) by using $[Cu_{20}H_{11}\{S_2P(C_2H_4Ph)_2\}_9]$[16] as the starting reagent. The molecular ions [**2a**$^+$], [**2b**$^+$**]** and [**2c**$^+$] appear at m/z 2642.10 (calcd 2642.37), m/z 2642.39 (calcd 2642.37), and 3196.49 (calcd 3195.63), respectively, and there is a good match between their experimental and simulated isotopic patterns (Figures S6-S8). In the negative-ion mode ESI-MS, a unique counteranion band is observed in the case of **2a**$^+$, corresponding to $(CuCl_2)^-$ (m/z 134.9; calcd 134.8; Figure S9). The ^1H and ^{13}C NMR spectra of **2a**$^+$, **2b**$^+$ and **2c**$^+$ show similar NMR patterns with one type of alkyl dithiophosph(in)ate and alkynyl ligand signal, indicating highly symmetric structures in solution (Figures S10-S15). This is also supported by their ^{31}P NMR spectra: **2a**$^+$ at 101.73 ppm, **2b**$^+$ at 107.09 ppm, and **2c**$^+$ at 81.09 ppm (Figure S16-S18). These results are consistent with the fact that all the dithiolate and alkynyl ligands bind similarly to the $Au@Cu_{12}$ kernel, as in **1a**$^+$. The FT-IR spectra of clusters **2a**$^+$, **2b**$^+$, and **2c**$^+$ exhibit $\nu(PhC{\equiv}C^-)$ stretching frequencies at 2014.3 (**2a**$^+$), 2018.9 (**2b**$^+$) and 1968.0 (**2c**$^+$) cm^{-1} (Figure S19-S21), which are lower than the value of the free phenylacetylene ligand ($\nu_{C\equiv C}$ = 2110 cm^{-1}).

A similar synthetic procedure was conducted to obtain compound **3**(PF_6). An equimolar amount of $[Ag(CH_3CN)_4](PF_6)$ was added to the THF suspension of copper(I) hydride $[Cu_{30}H_{18}\{S_2P(O^nPr)_2\}_{12}]$[15] along with eighteen equiv. of phenylacetylene. The reaction was stirred for 48 hours at 30 °C. Purification of reaction products led to the isolation of

$[AgCu_{12}\{S_2P(O^nPr)_2\}_6(C{\equiv}CPh)_4]^+$ (**3**$^+$) as a dark magenta precipitate in 29% yields. A band for [**3**$^+$] at m/z 2554.30 (calcd 2554.30), consistent with its simulated isotopic pattern, is identified in the positive-ion ESI mass spectrum of compound **3** (Figures S22). The ^{31}P NMR signal of **3**$^+$ was observed at 105.71 ppm and that of its counterion PF_6^- at -142.67 ppm, with a septet pattern (Figure S23). Similar to clusters [**1**$^+$] and [**2**$^+$], only one type of alkyl ligand is found in the ^{1}H and ^{13}C NMR spectra (Figure S24-S25). The FT-IR spectrum exhibits ν(PhC≡C$^-$) stretching frequencies at 2015.0 cm^{-1} (Figure S26), similar to that reported for $[Ag@Cu_{12}\{S_2CN^nBu_2\}_6(C{\equiv}CPh)_4]^+$ (2015 cm^{-1}).[11]

Because in the above clusters, the 13 metal atoms have a +11 global oxidation state (2-electron superatoms), the reactions in Scheme 1 correspond to a partial reduction of the heterometal. The Au(I) or Ag(I) salts are reduced by the hydrides of the starting copper(I) hydrides, as evidenced by the production of H_2, which can be detected by ^{1}H NMR spectroscopy during the reaction process. This route has been demonstrated in the fabrication of the 2-electron copper superatom, $[Cu_{13}H_2(dtc)_6(alkynyl)_4]^+$, via the degradation of an intermediate cluster, $[Cu_{15}H_2(dtc)_6(alkynyl)_6]^+$.[17]

Structural Analysis

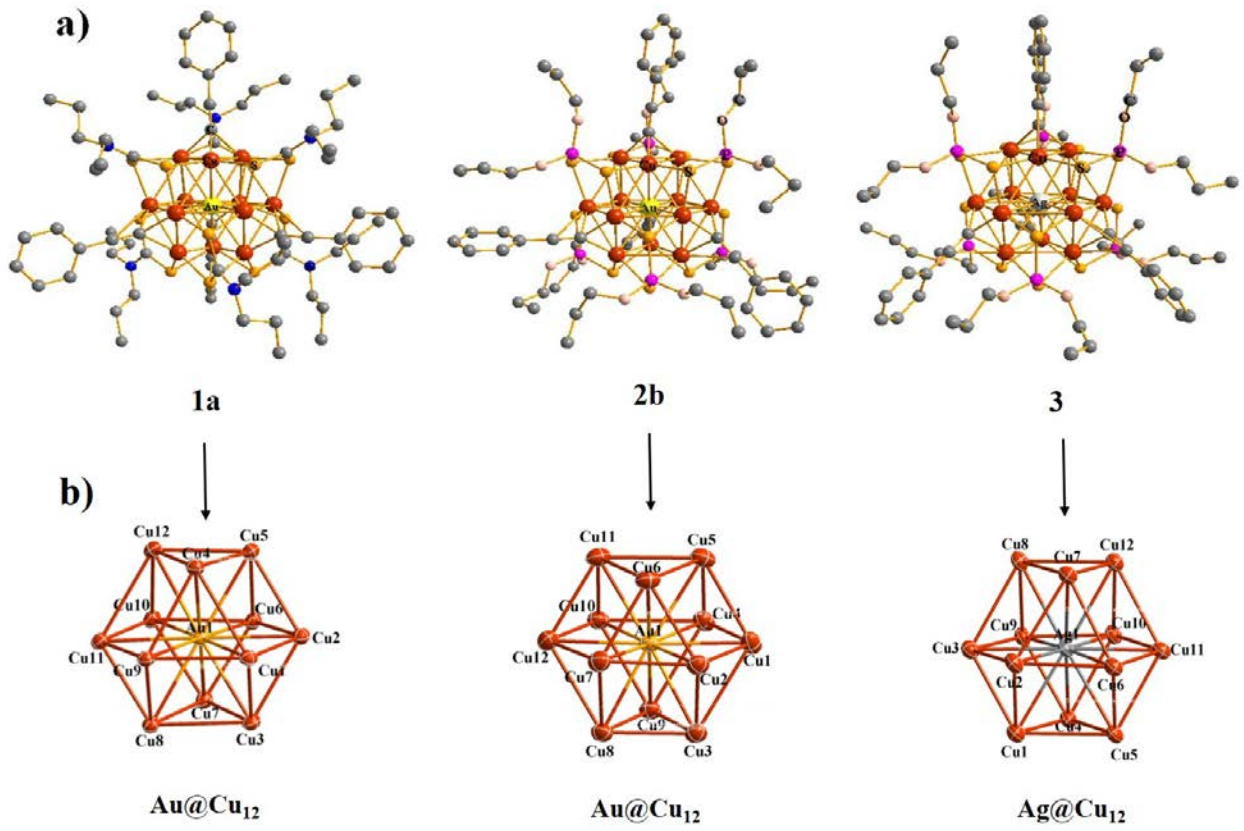

Figure 1. (a) Single crystal X-ray structures of cluster cations **1a**$^+$, **2b**$^+$, and **3**$^+$ with hydrogen atoms omitted for clarity; (b) Thermal ellipsoid drawings (50% probability) of centered cuboctahedral kernels M@Cu_{12} (M = Au, Ag).

Clusters **1a**$^+$ and **2a**$^+$ were isolated as salts of $[CuCl_2]^-$ with $P2_1/c$ and $P2_1/n$ space groups, respectively. **2b**$^+$ and **3**$^+$ crystallized with Cl^- (space group $P(-)1$) and PF_6^- (space group $P2_1/n$) counteranions, respectively. The X-ray structures of **1a**$^+$, **2a**$^+$, **2b**$^+$**,** and **3**$^+$ are similar to that of $[Au@Cu_{12}\{S_2CN^nBu_2\}_6(C{\equiv}CPh)_4]^+$ (**1b**$^+$),[11] as exemplified by the structural drawings of **1a**$^+$, **2b**$^+$, and **3**$^+$, as shown in Figure 1. They all exhibit an M-centered Cu_{12} cuboctahedron, the six square faces of which are capped by the six dithiolato ligands in a (μ_2, μ_2) binding mode and its four triangular faces by the four alkynyl ligands in a (μ_3-η^1) binding mode. Selected metric data of **1a**$^+$, **2a**$^+$, **2b**$^+$**,** and **3**$^+$ are given in Table 1, together with that of **1b**$^{+11}$ for comparison. Not considering their alkyl and phenyl substituents, all the complexes have idealized T_d symmetry. Their averaged M_{cent}-Cu and Cu_t-Cu distances are almost equal, although the latter can be divided into two groups. The dithiocarbamate derivatives **1a**$^+$ and **1b**$^+$ have metal-metal distances (~2.74 Å) slightly shorter than their dithiopho(phin)ate counterparts **2a**$^+$, **2b**$^+$**,** and **3**$^+$ (2.76-2.77

Å). This trend results from the smaller dithiocarbamate "bite distance" compared to that of a dithiophosph(in)ate. The Cu-S distances are slightly shorter in the case of the dithiocarbamate ligands. The Cu-C distances increase slightly in the order **1** > **2** > **3**. Overall, the five structures are quite similar.

Table 1. Selected bond lengths (Å) for **1a**$^+$, **1b**$^+$, **2a**$^+$, **2b**$^+$, and **3**$^+$.

	M_{cent}-Cu	Cu-Cu	Cu-S	Cu-C	C≡C
1a$^+$	2.7143(11)-2.7533(11) avg. 2.7356(11)	2.5018(13)-2.9546(13) avg. 2.7352(13)	2.265(2)-2.332(2) avg. 2.290(2)	2.011(8)-2.103(7) avg. 2.046(8)	1.199(11)-1.234(10) avg. 1.215(11)
1b$^+$ [11]	2.7102(7)-2.7735(7) avg. 2.7336(7)	2.5283(9)-2.9134(9) avg. 2.7337(9)	2.2638(14)-2.3208(15) avg. 2.2927(15)	1.971(5)-2.089(5) avg. 2.037(6)	1.208(8)-1.218(7) avg. 1.213(8)
2a$^+$	2.7575(11)-2.7942(10) avg. 2.7733(11)	2.5499(14)-3.0291(14) avg. 2.7723(14)	2.296(2)- 2.334(3) avg. 2.313(3)	2.005(9)-2.081(9) avg. 2.030(9)	1.192(12)-1.218(12) avg. 1.208(12)
2b$^+$	2.7380(11)-2.7866(11) avg. 2.7641(11)	2.5730(14)-2.9248(15) avg. 2.7631(15)	2.283(3)-2.340(3) avg. 2.312(3)	2.003(10)-2.079(10) avg. 2.031(10)	1.197(13)-1.211(12) avg. 1.205(13)
3$^+$	2.7394(6)-2.7916(7) avg. 2.7636(7)	2.5416(8)-2.9022(8) avg. 2.7629(8)	2.2938(13)-2.3325(12) avg. 2.3178(13)	1.965(5)-2.080(4) avg. 2.018(5)	1.208(6)-1.220(6) avg. 1.214(6)

X-ray Photoelectron Spectroscopy

The oxidation state of the central metal in the cluster was evaluated by X-ray photoelectron spectroscopy (XPS). The XPS spectrum exhibits an Au $4f_{7/2}$ peak for clusters **1a**$^+$ (83.68 eV), **2a**$^+$ (83.98 eV), **2b**$^+$ (83.88 eV), and **2c**$^+$ (84.08 eV) (Figure S27-S30). These values are close to that of bulk Au metal (84.0 eV). They are echoed by the previously DFT-calculated natural atomic orbital (NAO) charge of Au, -0.81, on the model $[Au@Cu_{12}(S_2CNH_2)_6(C{\equiv}CH)_4]^+$.[11] They are, however, lower than those reported for the alleged Au(0) clusters $Au_2Cu_6(PPh_2Py)_2(SC_{10}H_{15})_6$ (84.29 eV) and $Au_{15.37}Cu_{16.63}$(S-Adm)$_{20}$ (84.30 eV) reported by Zhu et al.[5a,8a,18]

A similar trend is found in the Ag $3d_{5/2}$ binding energy of cluster **3**$^+$ (367.8 eV, see Figure S31), which is intermediate between that of Ag metal (368.2 eV) and that of Ag(I) (367.5 eV). The XPS features of all other elements were found exactly as expected (Figure S32-S36).

Optical Properties

The UV-vis absorption spectra of compounds **1a**($CuCl_2$), **2a**($CuCl_2$), **2b**(Cl), **2c**($CuCl_2$), and **3**(PF_6) are shown in Figure 2. Their corresponding λ_{max} values are listed in Table 2, together with that of (**1b**)($CuCl_2$)[11] for comparison. They exhibit remarkably similar optical features. Those of $\mathbf{1a}^+$ and $\mathbf{1b}^+$ (gold/dithocarbamates) are very close, as are those of $\mathbf{2a}^+$ and $\mathbf{2b}^+$ (gold/dithiophophates). Those of **2c** (gold/dithiophosphate) are closer to those of $\mathbf{2a}^+$ and $\mathbf{2b}^+$. A similar tendency can be noticed for **3** (silver/dithiophophates). Thus, a significant hypsochromic shift in the lowest energy band when going from dithiocabamate to dithiophosph(in)ate ligands can be traced. Since the low-energy band is a HOMO (1S)→LUMO (1P) transition,[11] it follows that this gap is slightly larger in the case of dithiophosph(in)ate ligands than in the case of dithiocarbamates. This is in line with the fact that in the case of the dithiocarbamate series, the 1P LUMOs are somewhat stabilized by π*(CN) levels.[11] With respect to the high-energy band, an opposite (bathochromic) shift is observed upon going from dithiocabamate to dithiophosph(in)ate ligands. Since $\mathbf{2b}^+$ and $\mathbf{3}^+$ differ only by the nature of their heterometal (Au or Ag), it is possible to evaluate their effect on the absorption features. It appears that the effect is negligible on both the low- and high-energy absorption bands. This result is somewhat surprising because DFT calculations on related models found a significantly larger HOMO-LUMO gap for gold-centered species.[11] A reasonable explanation is that in the case of **3**, the low-energy band is associated with a HOMO → LUMO transition that is mixed with another transition of higher energy.

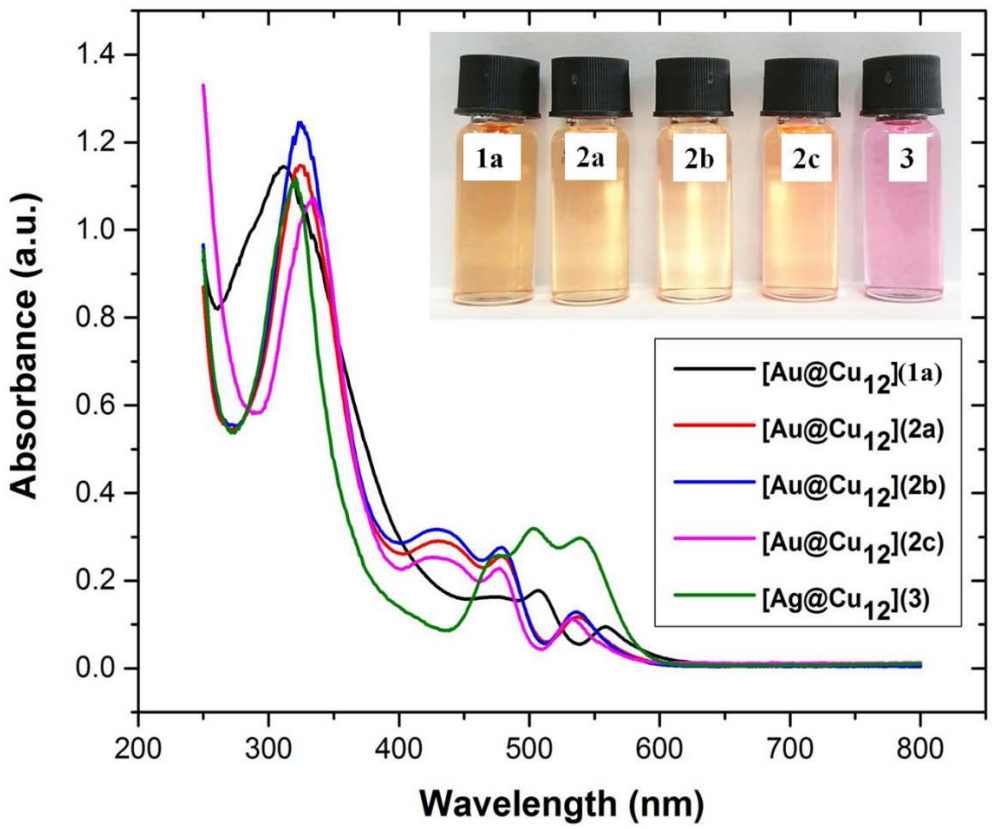

Figure 2. UV-vis absorption spectra of salts of $\mathbf{1a}^+$, $\mathbf{2a}^+$, $\mathbf{2b}^+$, $\mathbf{2c}^+$, and $\mathbf{3}^+$ in CH_2Cl_2. The inset shows photographs in CH_2Cl_2 at ambient temperature.

The stability of the bimetallic alloys was evaluated by time-dependent UV-vis absorption spectroscopy and recorded at 20°C in dichloromethane. The UV-vis spectra of $\mathbf{1a}^+$ revealed only a minor change after 28 days (Figure S37), while the absorption profiles of $\mathbf{2a}^+$, $\mathbf{2b}^+$, and $\mathbf{2c}^+$ did not change over 28 days (Figure S38-S40). The UV-vis spectra of $\mathbf{3}^+$ changed steadily over time, and the cluster was completely decomposed within 8 days (Figure S41). Based on these observations, alloy $\mathbf{1}^+$ is less stable than alloy $\mathbf{2}^+$, for which the exact reasons are still unknown. The bimetallic gold-centered, copper-rich clusters have enhanced stability relative to the Ag analog.

Luminescence Properties

Bimetallic clusters, $\mathbf{1}^+ \sim \mathbf{3}^+$, exhibit strong photoluminescence at ambient temperature in both solution (in MeTHF) and the solid-state. As shown in Figures S43-S48, each cluster has a

one-exponential fitting lifetime falling on the microsecond scale in solution at room temperature (Table 2). Such long emission lifetimes strongly suggest the emissive origin to be from a spin-forbidden triplet excited state. The emission profiles of $\mathbf{1}^+ \sim \mathbf{3}^+$ are shown in Figures 3 and S42. The photophysical data of their respective salts recorded at 298 K are summarized in Table 2 together with those of (**1b**)($CuCl_2$)[11] for comparison. Previously, we reported that $\mathbf{1b}^+$ emits intense red light with an emission wavelength centered at λ_{em} = 616 nm (λ_{exc} = 473 nm) at 77 K in solution, where the quantum yield achieves 59%.[11] For the emission λ_{max} values, the room temperature λ_{em} values reported in Table 2 for clusters $\mathbf{1}^+$-$\mathbf{3}^+$ in solution can also be divided into 4 groups, namely, ($\mathbf{1a}^+$, $\mathbf{1b}^+$), ($\mathbf{2a}^+$, $\mathbf{2b}^+$), $\mathbf{2c}^+$ and $\mathbf{3}^+$. Within the gold-derivative series (clusters $\mathbf{1}^+$-$\mathbf{2}^+$), the hyposchromic shift observed in the low-energy emission upon going from the dithiocarbamate to the dithiophosph(in)ate ligands is also operative, in line with a larger HOMO-LUMO gap for the dithiophosph(in)ate species. The significantly larger emission wavelength (762 nm) observed for Ag-centered alloy $\mathbf{3}^+$, compared to its Au relative $\mathbf{2b}^+$ (642 nm), is in line with previous DFT-computed HOMO-LUMO gaps found for simplified related model clusters.[11]

In the solid-state (Figure S42), the room temperature emission wavelengths of $\mathbf{2a}^+$, $\mathbf{2b}^+$ and $\mathbf{2c}^+$ (623, 638 and 617, respectively) barely change compared to their solution counterparts. In the cases of $\mathbf{1a}^+$ and $\mathbf{1b}^+$, it is redshifted to 724 and 765 nm, respectively. This behavior could be tentatively explained by the availability in $\mathbf{1a}^+$ and $\mathbf{1b}^+$ of the π^*(dithiocarbamate) orbitals. These MOs, which are situated not far above the three superatomic 1P LUMOs,[11] could, by simple C=N stretching, stabilize a low-lying triplet state that would be radiatively emitting only in the solid-state.

Ranging from 23% ($\mathbf{1a}^+$) to 55% ($\mathbf{2b}^+$), the QY reported in Table 2 is substantial for all gold-centered species. The much lower value obtained for **3** is consistent with the expected small spin-orbit coupling in the case of silver, as opposed to the heavier gold element, for which it favors spin intersystem crossing.[19] This result is also consistent with the fact that the Au-centered species exhibit significantly shorter PL lifetimes than the Ag-centered cluster. Going down to Cu renders spin-orbit coupling even more negligible, and consistently, $[Cu@Cu_{12}\{S_2CN^nBu\}_2(C{\equiv}CPh)_4](CuCl_2)$ displays a very weak emission in the NIR region in a 2-MeTHF solution at 77 K and no emission at all at ambient temperature.[11] The results indicate that the PLQY for the two-electron bimetallic alloy clusters follows the order $Au@Cu_{12}$> $Ag@Cu_{12}$ >> $Cu@Cu_{12}$. Thus, gold doping is an efficient method for boosting the luminescent QY of bimetallic Cu-rich alloys,

and the fact that the Au@Cu_{12} series has faster phosphorescence k_{RAD} amplitudes than that of Ag@Cu_{12} species (see Table 2) can be attributed to the heavy atom effect.[19]

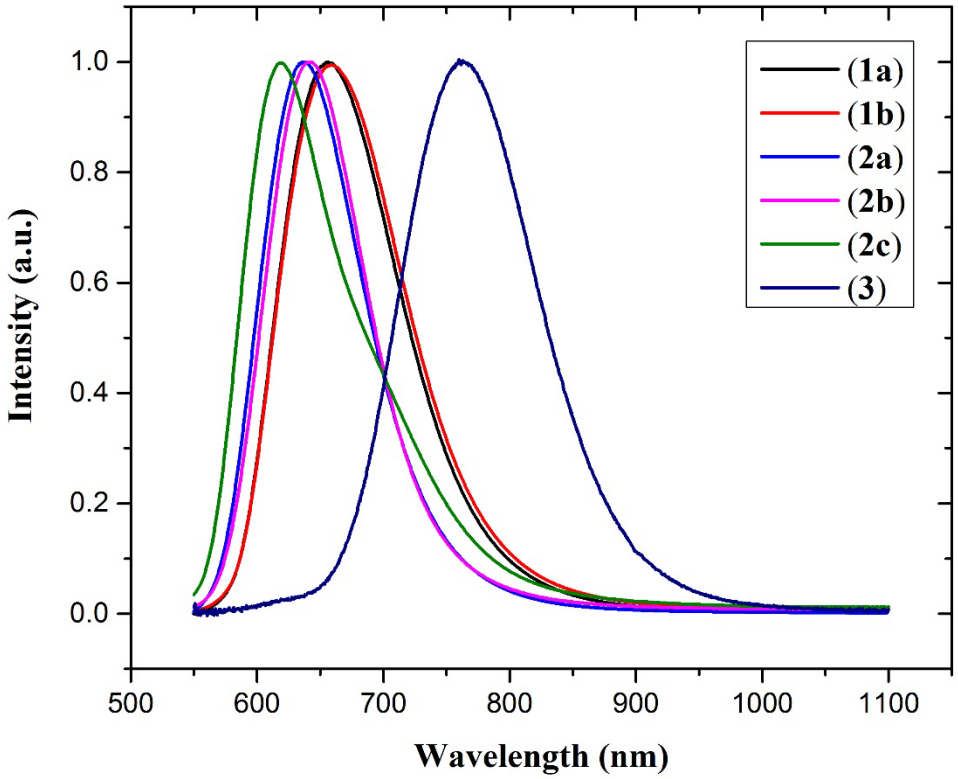

Figure 3. Emission spectra of **1a**$^+$, **1b**$^+$, **2a**$^+$, **2b**$^+$, **2c**$^+$, and **3**$^+$ in MeTHF at ambient temperature.

Whereas the solutions of dithiocarbamate species **1a**$^+$ and **1b**$^+$ have the largest radiative rate constant, they also have the largest nonradiative rate constant (together with **2c**$^+$). With its lowest nonradiative rate constant, **2b**$^+$ reaches the highest QY. Among the four gold-centered species, **2b**$^+$ is the only one having chloride as a couteranion, and the others have a complex anion $(CuCl_2)^-$. An explanation (among others) for the limited nonradiative processes in **2b**$^+$ is that the specific interactions with the chloride couteranion in the excited state could limit the nonradiative decay by enhancing the rigidity. More experiments with various salts of various gold/dithiophosphate relatives are needed to obtain a better understanding of the PL efficiency.

Table 2. 298 K absorption, emission, and lifetime of **1a**$^+$, **1b**$^+$, **2a**$^+$, **2b**$^+$, **2c**$^+$, and **3**$^+$ in 2-MeTHF

Compound	λ_{max}(nm) [$\varepsilon(M^{-2a}m^{-1})$]	λ_{em} (nm)	Lifetime, $\tau(\mu s)$ One-exp[a]	Φ_{em}[b]	k_{obs}, $1/\tau(\mu s^{-1})$; one-exp	k_{RAD}[c] (μs^{-1})	k_{NRD}[d] (μs^{-1})
1a($CuCl_2$)	311, 475, 508, 560 [8150]	657	0.76	0.23	1.3	0.30	1.0
1b($CuCl_2$)[11]	310, 476, 509, 561 [6400]	658	1.41	0.43	0.710	0.31	0.40
2a($CuCl_2$)	326, 433 480,540 [8510]	637	3.20	0.32	0.31	0.10	0.21
(2b(Cl)	324, 427, 480, 536 [5310]	642	3.67	0.55	0.27	0.15	0.12
2c($CuCl_2$)	333, 427, 477, 533 [8340]	618	1.86	0.25	0.53	0.13	0.40
3(PF_6)	321, 476, 503, 537 [11700]	762	14.7	0.058	0.068	0.0039	0.064

[a] mean emission lifetime (τ). [b] emission quantum yield (see page S1(SI)). [c] $\Phi_{em}= k_{RAD}/k_{obs}$, k_{RAD} = radiative rate constant and k_{obs} = mean excited-state decay rate constant. [d] $k_{obs} = k_{RAD} + k_{NRD}$, k_{NRD} = nonradiative rate constant. [e] 77 K emission in 2-MeTHF glasses, weak emission intensity.

Electrochemical Investigations

The electrochemical behavior of clusters $\mathbf{1}^+$-$\mathbf{3}^+$ was investigated in CH_2Cl_2 solution at 233 K. The results, shown in Figures 4, S49 and S50, are summarized in Table 3. Cyclic voltammograms (CVs) and differential pulse voltammograms (DPVs) of dithocarbamate species $\mathbf{1a}^+$ and $\mathbf{1b}^+$ display one irreversible reduction process (E_{pc}) at approximately –2.15 V and four quasi-reversible oxidation processes (E_{pa}) between -0.21 and +0.57 V. In the case of dithiophosphate derivatives $\mathbf{2a}^+$ and $\mathbf{2b}^+$, the reversibility of the redox processes is improved,

with two quasi-reversible E_{pc} waves in the same region and two E_{pa} oxidations, in which the second process is quasi-reversible. Dithiophosphinate species **2c**$^+$ exhibits one E_{pc} wave and three E_{pa} processes, of which the second is quasi-reversible. Regarding **3**$^+$, the Ag analog of **2b**$^+$, two irreversible reductions and four oxidations, of which the second is quasi-reversible, are recorded. From previous DFT calculations on related simplified models,[11] the reduction should correspond to electron transfer into the triply degenerate 1P LUMO, and the first two one-electron oxides should concern the 1S HOMO. The mono- and di-oxidized species were computed to be thermally stable. According to the results of the electrochemical study, the di-oxidized species is more stable than the mono-oxidized species.

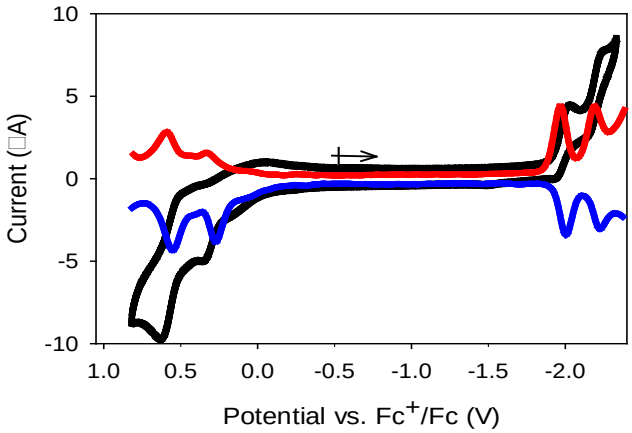

Figure 4. Cyclic voltammogram (black) and differential pulse voltammograms (blue and red line) of **2a**$^+$ (0.6 mM) at 233 K in CH_2Cl_2 containing 0.1 M [^{n}Bu$_4$N][B(C$_6$F$_5$)$_4$] solution under N_2 atmosphere.

The Au-centered clusters exhibit higher stability in the reduced state relative to the Ag-doped derivative. Regarding the ligand influence, the dithiocarbamate-ligated clusters display greater susceptibility toward decomposition upon redox events. This observation is consistent with the results of time-dependent electronic spectra, revealing faster decay of the dithiocarbamate clusters compared with the corresponding dithiophosph(in)ate derivatives. The resulting electrochemical HOMO-LUMO gaps (E^E_g) are all approximately 2 eV (Table 3), and that of Ag derivative **3** is definitely lower than that of its Au congeners. These values are consistent with the optical HOMO-LUMO gaps computed from the lowest energy absorption band λ_{max} values (E_g^O) as well as those computed from the recorded PL λ_m values (E_g^{PL}). The only inconsistent value is that of E_g^O for **3**$^+$, for which we suspect that the λ_{max} transition is not

associated with a pure HOMO→LUMO transition (see above). Indeed, DFT-computed HOMO-LUMO gaps on related species support the view of lower HOMO-LUMO gaps in the case of Ag-centered species.[11] Within the Au-centered series, the increasing HOMO-LUMO gaps in the order **2c**$^+$ > (**2a**$^+$, **2b**$^+$) > (**1a**$^+$, **1b**$^+$) are fully consistent with the variation of the PL λ_{em} wavelength, as well as the lowest optical λ_{max} value.

Table 3. Summary of redox potentials (V vs Fc^+/Fc) and estimated band gaps (eV) of compounds **1-3**.

Cluster	E_{pa}[†]	E_{pc}[†]	E_g^E [§]	E_g^O [§]	E_g^{PL} [§]
1a$^+$	–0.12, +0.17, +0.37, +0.57	–2.14	2.02	2.21	1.89
1b$^{+,\,11}$	–0.21, +0.12, +0.25, +0.54	–2.15	1.94	2.21	1.89
2a$^+$	+0.26, +0.56[‡]	–1.96[‡], –2.19[‡]	2.22	2.30	1.95
2b$^+$	+0.16, +0.65[‡]	–1.95[‡], –2.17[‡]	2.11	2.31	1.93
2c$^+$	+0.19, +0.58[‡], +0.82	–2.04	2.23	2.33	2.01
3$^+$	–0.07, +0.15[‡], +0.55, +0.76	–1.95, –2.16	1.88	2.31	1.63

[†]Potentials were determined by DPV. The measurements were collected at 233 K. All redox processes are irreversible unless they are labeled as ‡, indicating quasi-reversible processes. [§]E_g^E and E_g^O are the electrochemical and optical HOMO-LUMO gaps, respectively. $E_g^E = E_{pc} - E_{pa}$, and $E_g^O = 1240/\lambda_{max}$, where λ_{max} (in mm) corresponds to the lowest electronic transition. $E_g^{PL} = 1240/\lambda_{em}$ where λ_{em} (in mm) is the PL wavelength. [‡]Quasi-reversible.

Conclusions

In summary, we report a new synthetic procedure for the preparation of atomically precise gold- and silver-doped copper 2-electron clusters of the type $[M@Cu_{12}(dithiolate)_6(C{\equiv}CPh)_4]^+$, where the dithiolate is dithiocarbamate, dithiophosphate, or dithiophosphinate. Five new types of compounds were synthesized and fully characterized from the reaction of various copper(I) hydrides with phenylacetylene in the presence of Au(I) or Ag(I) salts. These 2-electron clusters of ideal T_d symmetry have a gold- (or silver-) centered Cu_{12} cuboctahedral core protected by six dithiolate and four alkynyl ligands. UV-vis, PL, and electrochemical experiments are consistent with a HOMO-LUMO gap depending on the dithiolate nature and increasing in the order dithiophosphinate > dithiophosphate > dithiocarbamate. The silver-centered cluster appears to behave somewhat differently from its gold-centered relatives: whereas the latter exhibits good PL efficiency, the former only weakly emits. The largest recorded QY (55%) was obtained for one of the gold-centered dithiophosphate derivatives, which are the most thermally stable among the investigated families. Further research is planned to design new salts of $[Au@Cu_{12}(dithiolate)_6(C{\equiv}CPh)_4]^+$ cationic clusters to enhance their QY and tune their emission wavelengths for various potential applications.

Experimental Section

All chemicals were purchased from commercial sources and used as received. Solvents were purified by following standard protocols. All reactions were performed in oven dried Schlenk glassware and carried out under N_2 atmosphere. The starting copper hydrides $[Cu_{28}H_{15}\{S_2CN^nPr_2\}_{12}](PF_6)$,[13] $[Cu_{20}H_{11}\{S_2P(O^iPr)_2\}_9]$,[14] $[Cu_{30}H_{18}\{S_2P(O^nPr)_2\}_{12}]$,[15] and $[Cu_{20}H_{11}\{S_2P(C_2H_4Ph)_2\}_9]$[16] were prepared by slightly modified procedures reported earlier in literature. NMR spectra were recorded on a Bruker Advance DPX300 FT-NMR spectrometer operating at 300 MHz. The chemical shifts (δ) and coupling constants (J) are reported in ppm and Hz, respectively. ^{31}P NMR spectra are referenced to external 85% H_3PO_4. ESI-mass spectra were recorded on a Fison Quattro Bio-Q (Fisons Instruments, VG Biotech, U. K.). XPR experiments were performed with an X-ray photoelectron spectrometer XPS, VG Multilab 2000-Thermo Scientific Inc. UK, Kα, with a microfocus monochromated Al Kα X-ray working with high photonic energies from 0.2 to 3 KeV. The room temperature absorption spectra in 2-MeTHF (2-Methyltetrahydrofuran) were recorded on a Shimadzu UV-3101PC

spectrophotometer. Emission spectra and lifetimes in solution were obtained in 2 mm cylindrical quartz cells in a spectroscopic quartz Dewar as described in elsewhere.[20-21] Emission spectra at room temperature were obtained by using a Xe lamp for wavelengths and an Oriel model 63358 or 63966 Quartz Tungsten Halogen (QTH) lamp for intensities. The emission spectra were collected using a HORIBA JOBIN YVON iHR 550 spectrometer with three gratings (300 l/mm, 600 nm blaze; 300 l/mm, 1 μm blaze; and 600 l/mm, 1 μm blaze) and a HORIBA Symphony InGaAs-1700 (for the NIR) detector head was mounted on the exit port. This system was operated through the SynerJY software. The detector heads was cooled to -90ºC and the spectrometers was purged with dry N_2. The room temperature emission lifetimes were determined using a LTB Model MNL 103-PD nitrogen laser-pumped, a LTB Model DUL 100 Dye laser system for excitation, a Hamamatsu P928 PMT/E717-63 socket assembly mounted on a Jobin-Yvon H-100 spectrometer for detection in the visible region and a Hamamatsu NIR-PMT Modul H10330A-75 for collection in the NIR region. Both detector systems for detection in the visible and NIR regions were output digitized using the LeCroy WaveRunner 6030A software. Electrochemical measurements were recorded on a CH Instruments 733B electrochemical potentiostat using a gastight three-electrode cell under N_2 at 273 K or 233 K. A vitreous carbon electrode (1 mm or 3 mm in diameter) and a platinum wire were used as working and auxiliary electrode, respectively. Reference electrode was a non-aqueous Ag^+/Ag electrode (0.01 M $AgNO_3$/0.1 M [*n*Bu_4N][$BArF_{24}$], $BArF_{24}^-$ = $B(3,5\text{-}C_6H_3(CF_3)_2)_4^-$). All experiments were measured in CH_2Cl_2 solutions with 1 mM analyte and 0.1 M [*n*Bu_4N][$BArF_{24}$] supporting electrolyte concentrations and were recorded at a 100 mV/s scan rate unless otherwise stated. The potentials are reported against the ferrocenium/ferrocene (Fc^+/Fc) couple.

Synthesis of 1a($CuCl_2$)**:**

In a flame-dried Shlenck tube, [$Cu_{28}H_{15}\{S_2CN^nPr_2\}_{12}$]($PF_6$), (0.1 g; 0.025 mmol) was suspended in THF (5 mL) along with Au(PPh_3)Cl (0.012 g; 0.025 mmol) and phenylacetylene (40 uL; 0.375 mmol), the resulting mixture was stirred at 30°C for 48 hours. The solvent was evaporated under vacuum and residue washed with diethyl ether (3x15 mL) to remove impurities from the ligands. The red residue was extracted in methanol and passed through Al_2O_3. Finally, the solvent was evaporated to dryness under vacuum to get a pure dark red powdered **1a**($CuCl_2$) in

0.052 g (38.35 % based on Cu) yields. In this reaction, corresponding alkenes and $[Cu_8H\{S_2CN^nPr_2\}_6]^+$ has been produced as by products.

1a($CuCl_2$): ESI-MS: *m/z* 2420.60 (M^+), 134.90 (M^-). ^{1}H NMR (300 MHz, $CDCl_3$): 7.26-7.49 (20H, C_6H_5), 3.82 (24H, NCH_2), 1.70 (24H, CH_2), 0.86 (36H, CH_3) ppm; ^{13}C NMR (100.61 MHz, $CDCl_3$): 203.26, 131.98, 128.28, 123.79, 77.81, 77.30, 59.53, 20.45, 11.19; FT-IR data in CsI pellet (cm^{-1}); 2962.4, 2932.5, 2873.3, 2018.7, 1592.3, 1304.9, 1238.8, 940.4, 893.8. Anal. Calcd for $C_{74}H_{104}AuCl_2Cu_{13}N_6S_{12}$: C, 34.77; H, 4.10; N, 3.29; S, 15.05. Found: C, 33.21; H, 4.22; N, 3.92; S, 14.68

Synthesis of 2a($CuCl_2$)**:**

In a flame-dried Shlenck tube, $[Cu_{20}H_{11}\{S_2P(O^iPr)_2\}_9]$ (0.1 g; 0.031 mmol) was suspended in THF (5 mL) along with $Au(PPh_3)Cl$ (0.015 g; 0.031 mmol) and phenylacetylene (40 uL; 0.341 mmol), the resulting mixture was stirred at 30°C for 48 hours. The solvent was evaporated under vacuum and residue washed with diethyl ether (3x15 mL) to remove impurities from the ligands. The red residue was extracted in methanol and passed through Al_2O_3. Finally, the solvent was evaporated to dryness under vacuum to get a pure red powdered **2a**($CuCl_2$) in 0.058 g (43.44 % based on Cu) yields. In this reaction, corresponding alkenes and $[Cu_8H\{S_2P(O^iPr)_2\}_6]^+$ has been produced as by products.

2a($CuCl_2$): ESI-MS: *m/z* 2642.10 (M^+), 134.90 (M^-). ^{1}H NMR (300 MHz, $CDCl_3$): 7.60-7.61 (20H, C_6H_5), 4.82 (12H, OC*H*), 1.17 (72H, CH_3) ppm; ^{13}C NMR (100.61 MHz, $CDCl_3$): 132.82, 128.27, 123.79, 75.80, 74.83, 53.84, 23.26 ppm; ^{31}P NMR (121.49 MHz, $CDCl_3$); 101.73 ppm; FT-IR data in CsI pellet (cm^{-1}); 2979.7, 2932.8, 2872.3, 2014.3, 1592.3, 1261.6 951.7, 887.0. Anal. Calcd for $C_{68}H_{104}AuCl_2Cu_{13}O_{12}P_6S_{12}$: C, 29.40; H, 3.77; O, 6.91; S, 13.85. Found: C, 29.27; H, 3.57; O, 6.75; S, 13.70.

Synthesis of 2b(Cl)**:**

In a flame-dried Shlenck tube, $[Cu_{30}H_{18}\{S_2P(O^nPr)_2\}_{12}]$, (0.05 g; 0.01 mmol) was suspended in THF (5 mL) along with $Au(PPh_3)Cl$ (0.005 g; 0.01 mmol) and phenylacetylene (25 µL; 0.18 mmol), the resulting mixture was stirred at 30°C for 48 hours. The solvent was evaporated under vacuum and residue washed with diethyl ether (3x15 mL) to remove impurities from the ligands. The red residue extracted in methanol and passed through Al_2O_3. Finally, the solvent was

evaporated to dryness under vacuum to get a pure red powdered **2b**(Cl) in 0.049 g (41.56 % based on Cu) yields. In this reaction, corresponding alkenes and $[Cu_8H\{S_2P(O^nPr)_2\}_6]^+$ have been produced as by products.

2b(Cl): ESI-MS: *m/z* 2642.39 (M^+). ^{1}H NMR (300 MHz, $CDCl_3$): 7.33-7.56 (20H, C_6H_5), 3.97 (24H, OCH_2), 1.36 (24H, CH_2), 0.75 (36H, CH_3) ppm; ^{13}C NMR (100.61 MHz, $CDCl_3$): 132.11, 128.48, 122.79, 72.08, 71.51, 23.16, 10.05 ppm; ^{31}P NMR (121.49 MHz, $CDCl_3$); 107.09 ppm; FT-IR data in CsI pellet (cm^{-1}); 2969.1, 2937.3, 2879.2, 2018.9, 1593.1, 1200.0, 912.3, 844.4. Anal Calcd for $C_{68}H_{104}AuClCu_{12}O_{12}P_6S_{12}$: C, 30.49; H, 3.91; S, 14.36. Found: C, 33.11; H, 4.22; S, 14.60.

Synthesis of 2c($CuCl_2$)**:**

In a flame-dried Shlenck tube, $[Cu_{20}H_{11}\{S_2P(C_2H_4Ph)_2\}_9]$, (0.1 g; 0.025 mmol) was suspended in THF (5 mL) along with $Au(PPh_3)Cl$ (0.012 g; 0.025 mmol) and phenylacetylene (30 uL; 0.275 mmol), the resulting mixture was stirred at 30°C for 48 hours. The solvent was evaporated under vacuum and residue was washed with diethyl ether (3x15 mL) to remove impurities from the ligands. The red residue was extracted in methanol and passed through Al_2O_3. Finally, the solvent was evaporated to dryness under vacuum to get a pure powdered **2c**($CuCl_2$) in 0.066 g (49.39 % based on Cu) yields. In this reaction, corresponding alkenes and $[Cu_8H\{S_2P(C_2H_4Ph)_2\}_6]^+$ have been produced as by products.

2c($CuCl_2$): ESI-MS: *m/z* 3196.49 (M^+). ^{1}H NMR (300 MHz, $CDCl_3$): 6.70-7.19 (80H, C_6H_5), 2.86 (24H, PCH_2), 2.55 (24H, CH_2) ppm; ^{13}C NMR (100.61 MHz, $CDCl_3$): 139.04, 131.55, 128.90, 128.78, 127.90, 126.70, 121.43, 77.39, 74.04, 34.55, 30.69 ppm; ^{31}P NMR (121.49 MHz, $CDCl_3$); 81.9 ppm; FT-IR data in CsI pellet (cm^{-1}); 3060.4; 3027.4, 2929.9, 2861.0, 1968.0. Anal. Calcd for $C_{128}H_{128}AuCl_2Cu_{13}P_6S_{12}$: C, 46.16; H, 3.87; S, 11.55. Found: C, 46.93; H, 4.04; S, 11.20.

Synthesis of 3(PF_6)**:**

In a flame-dried Shlenck tube, $[Cu_{30}H_{18}\{S_2P(O^nPr)_2\}_9]$, (0.045 g; 0.01 mmol) was suspended in THF (5 cm^3) along with $[Ag(CH_3CN)_4](PF_6)$ (0.004 g; 0.01 mmol) and phenylacetylene (20 uL; 0.18 mmol), the resulting mixture was stirred at 30°C for 72 hours. The solvent was evaporated under vacuum and residue washed with diethyl ether (3x15 mL) to

remove impurities from the ligands. The black residue was extracted in methanol and passed through Al_2O_3. Finally, the solvent was evaporated to dryness under vacuum to get a pure black powdered **3**(PF_6) in 0.019 g (29.27 % based on Cu) yields. In this reaction, corresponding alkenes and $[Cu_8H\{S_2P(O^nPr)_2\}_6]^+$ have been produced as by products.

3(PF_6): ESI-MS: *m/z* 2554.30 (M^+). ^{1}H NMR (300 MHz, d_6-acetone): 7.46-7.67 (20H, C_6H_5), 4.07 (24H, OCH_2), 1.40 (24H, CH_2), 0.74 (36H, CH_3) ppm; ^{13}C NMR (100.61 MHz, $CDCl_3$): 132.17, 128.48, 122.76, 77.24, 72.06, 71.41, 23.11, 10.06 ppm; ^{31}P NMR (121.49 MHz, d_6-acetone); 105.70, -143.0 ($J_{P\text{-}F}$= 708.29 Hz) ppm; FT-IR data in CsI pellet (cm^{-1}); 2969.2, 2937.7, 2880.5, 2015.0, 1592.7, 1199.4, 913.1, 844.4. Anal. Calcd for $C_{68}H_{104}AgCu_{12}F_6O_{12}P_7S_{12}$: C, 30.26; H, 3.88. Found: C, 29.86; H, 3.84.

X-ray Crystallography

Single crystals suitable for X-ray diffraction analysis of salts of **1a**$^+$, **2a**$^+$, **2b**$^+$, and **3**$^+$ were obtained by slowly diffusing hexane into a concentrated acetone solution at -5 ºC temperature. The single crystals were mounted on the tip of glass fiber coated in paratone oil, then frozen at 150 K. Data were collected on a Bruker APEX II CCD diffractometer using graphite monochromated Mo Kα radiation (λ = 0.71073 Å). Data reduction was performed with SAINT,[22] Absorption corrections for the area detector were performed by using the SADABS program.[23] The structure was solved by direct methods and refined by least-squares against F2 using the SHELXL-97 package, [24] incorporated in SHELXTL/PC V5.10.6.[25] Selected Crystallographic data is given in Table S1.

Associated Content

Acknowledgment

This work was supported by the Ministry of Science and Technology in Taiwan (MOST 109-2113-M-259-008) and the France-Taiwan ANR-MOST 2018 program (project Nanoalloys).

References

1. Bootharaju, M. S.; Joshi, C. P.; Parida, M. R.; Mohammed, O. F.; Bakr O. M. Templated Atom Precise Galvanic Synthesis and Structure Elucidation of a

$[Ag_{24}Au(SR)_{18}]^-$ Nanocluster. *Angew. Chem. Int. Ed*. **2016**, *55*, 922–926; (b) Kang, X.; Li, Y.; Zhu, M.; Jin, R. Atomically precise alloy nanoclusters: syntheses, structures, and properties. *Chem. Soc. Rev.* **2020**, *49*, 6443-6514; (c) Kawawaki, T,; Imai, Y.; Suzuki, D.; Kato, S.; Kobayashi, I.;Suzuki, T.; Kaneko, R.; Hossain, S.; Negishi, Y. Atomically Precise Alloy Nanoclusters. *Chem. Eur. J.* **2020**, *26*, 166150-16193.

2. Barrabes, N.; Zhang, B.; Burgi, T. Racemization of chical $Pd_2Au_{36}(SC_2H_4Ph)_{24}$: doping increases the flexibility of the cluster surface. *J. Am. Chem. Soc*. **2014**, *136*, 14361−14364; (b) Yang, J.; Pang, R.; Song, D.; Li, M. –B. Tailoring silver nanoclusters via doping: advances and oppurtunities. *Nanoscale Adv*. **2021**, *3*, 2411-2422.
3. (a) Wang, Q.; Lee, Y.; Crespo, O.; Deaton, J.; Tang, C.; Gysling, H. J.; Gimeno, C.; Larraz, C.; Villacampa, M. D.; Laguna, A.; Eisenberg, R. Intensely luminescent gold(I)-silver(I) cluster complexes with tunable structural features. *J. Am. Chem. Soc.* **2004**, *126*, 9488-9489; (b) Kang, X.; Zhu, M. Tailoring the photoluminescence of atomically precise nanoclusters. *Chem. Soc. Rev.* **2019**, *48*, 2422-2457; (c) Yu, H.; Rao, B.; Jiang, W.; Yang, S.; Zhu, M. The photoluminescent metal nanoclusters with atomic precision. *Coor. Chem. Rev.* **201**9, *378*, 595-617.
4. (a) Xie, J.; Zheng, K.; Luo, Z. Engineering ultrasmall water-soluble gold and silver nanocluster for biomedical application. *Chem. Comm*. **2014**, *50*, 5143-5155; (b) Wang, S.; Meng, X.; Das, A.; li, T.; Song, Y.; Cao, T.; Zhu, X.; Zhu, M.; Jin, R. A 200-fold Quantum Yield Boost in the Photoluminescence of Silver-Doped AgxAu25-x Nanocluster: The 13 th Silver Atom Matters. *Angew. Chem. Int. Ed.* **2014**, *53*, 2376-2380; (c) Udayabhaskararao, T.; Sun, Y.; Gosmawi, N.; Pal, S. K.; Balasubramanian, K.; Pradeep, T. Ag_7Au_6: A 13-Atom Alloy Quantum Cluster. *Angew. Chem. Int. Ed*. **2012**, *51*, 2155-2159; (d) Tao, Y.; Li, M.; Ren, J.; Qu, X. Metal nanoclusters: novel probes for diagnostic and therapeutic applications. *Chem. Soc. Rev.* 2015, *44*, 8636-8663; (e) Song, X. –R.; Goswami, N.; Yang, H. –H.; Xie, J. Functionalization of metal nanocluster for biomedical applications. *Analyst*. **2016**, *141*, 3126-3140.
5. a) Kang, X.; Wang, S.; Song, Y.; Jin, S.; Sun, G.; Yu, H.; Zhu, M. Bimetallic Au_2Cu_6 Nanocluster: Strong Luminescence Induced by the Aggregation of Copper(I) with Gold(0) Species. *Angew. Chem. Int. Ed.* **2016**, *55*, 3611–3614. ; b) Kang, X.; Wang, S.; Zhu, M. Observation a new type of aggregation-induced emission in nanocluster. *Chem.*

Sci. **2018**, *9*, 3062-3068.; c) Dou, X.; Yuan, X.; Yu, Yong, Luo, Z.; Yao, Q.; Leong, D. T.; Xie, J. Lighting up thiolated Au@Ag nanoclusters via aggregation-induced emission. *Nanoscale*, **2014**, *6*, 157-161.

6. (a) Huang, R, -W.; Wei, Y. –S.; Dong, X. –Y.; Wu, X. –H.; Du, C. –X.; Zang, S. –Q.; Mak, T. C. W. Hypersensitive dual-function luminescence switching of a silver-chalcogenolate cluster-based metal-organic framework. *Nat. Chem*. **2017**, *9*, 689–697; (b) Huang, R.-W.; Dong, X.-Y.; Yan, B.-J.; Du, X.-S.; Wei, D.-H.; Zang, S.-Q.; Mak, T. C. W. Tandem Silver Cluster Isomerism and mixed Linkers to Modulate the Photoluminescence of Cluster-Assembled Materials. *Angew. Chem. Int. Ed.* **2018**, *57*, 8560–8566; (c) Dong, X.-Y.; Huang, H.-L.; Wang, J.-Y.; Li, H.-Y.; Zang, S.-Q. A Flexible Fluorescent SCC-MOF for Switchable Molecule Identification and Temperature Display. *Chem. Mater*. **2018**, *30*, 2160–2167.
7. (a) Dhayal, R. S.; Liao, J.-H.; Liu, Y.-C.; Chiang, M.-H.; Kahlal, S.; Saillard, J.-Y.; Liu, C. W. $[Ag_{21}\{S_2P(O^iPr)_2\}_{12}]^+$: an eight-electron superatom. *Angew. Chem. Int. Ed*. **2015**, *54*, 3702–3706; (b) Dhayal, R. S.; Lin, Y.-R.; Liao, J.-H.; Chen, Y.-J.; Liu, Y.-C.; Chiang, M.-H.; Kahlal, S.; Saillard, J.-Y.; Liu, C. W. $[Ag_{20}\{S_2P(OR)_2\}_{12}]$: A Superatom Complex with a Chiral Metallic Core and High Potential for Isomerism. *Chem. – Eur. J*. **2016**, *22*, 9943–9947; (c) Chang, W.-T.; Lee, P.-Y.; Liao, J.-H.; Chakrahari, K. K.; Kahlal, S.; Liu, Y.-C.; Chiang, M.-H.; Saillard, J.-Y.; Liu, C. W. Eight-Electron Silver and Mixed Gold/Silver Nanoclusters Stabilized by Selenium Donor Ligands. *Angew. Chem. Int. Ed.* **2017**, *56*, 10178-10182; (d) Lin, Y.-R.; Kishore, P. V. V. N.; Liao, J.-H.; Kahlal, S.; Liu, Y.-C.; Chiang, M.-H.; Saillard, J.-Y.; Liu, C. W. Synthesis, Structural Characterization and Transformation of an Eight-Electron Superatomic Alloy, $[Au@Ag_{19}\{S_2P(OPr)_2\}_{12}]$. *Nanoscale* **2018**, *10*, 6855-6860. (e) Xie, X.-Y.; Xiao, P.; Cao, X.; Fang, W.-H.; Cui, G.; Dolg, M. The Origin of the Photoluminescence Enhancement of Gold-Doped Silver Nanoclusters: The Importance of Relativistic Effects and Heteronuclear Gold-Silver Bonds. *Angew. Chem. Int. Ed*. **2018**, *57*, 9965–9969.
8. (a) Kang, X.; Li, X.; Yu.; Lv, Y.; Sun, G.; Li, Y.; Wang, S.; Zhu, M. Modulating photo-luminescence of Au_2Cu_6 nanocluster via ligand-engineering. *RSC. Adv*. **2017**, *7*, 28606-28609; (b) Gan, Z.; Lin, Y.; Luo, L.; Han, G.; Liu, W.; Liu, Z.; Yao, C.; Weng, L.; Liao,

L.; Chen, J.; Liu, X.; Luo, Y.; Wang, C.; Wei, S.; Wu, Z. Fluorescent Gold Nanoclusters with Interlocked Staples and a Fully Thiolate-Bound Kernel. *Angew. Chem. Int. Ed.* **2016**, *55*, 11567–11571; (c) Jin, S. Wang, S.; Xiong, L.; Zhou, M.; Chen, S.; Du, W.; Xia, A.; Pei, Y.; Zhu, M. Two-Electron Reduction: From Quantum Dots to Metal Nanoclusters. *Chem. Mater*. **2016**, *28*, 7905–7911.

9. Song, Y.; Weng, S.; Li, H.; Yu, H.; Zhu, M. The Structure of an Au_7Cu_{12} Bimetal Nanocluster and Its Strong Emission. *Inorg. Chem*. **2019**, *58*, 7136-7140.
10. Song, Y.; Li, Y.; Zhou, M.; Liu, X.; Li, H.; Wang, H,; Shen, Y.; Zhu, M.; Jin, R. Ultrabright $Au@Cu_{14}$ nanoclusters: 71.3% phosphorecescence quantum yield in non-degassed solution at room temperature. *Sci. Adv*. **2021**, *7*, eabd2091.
11. (a) Silalahi, R. P. B.; Chakrahari, K. K.; Liao, J.-H.; Kahlal, S.; Liu, Y.-C.; Chiang, M.-H.; Saillard, J.Y.; Liu, C. W. Synthesis of Two-Electron Bimetallic Cu-Ag and Cu-Au Clusters by Using $[Cu_{13}(S_2CN^nBu_2)_6(C{\equiv}CPh)_4]^+$ as a Template. *Chem. Asian J.,* **2018**. 13. 500-504. (b) Sharma, S.; Chakrahari, K. K.; Saillard, J.-Y.; Liu, C. W. *Structurally Precise Dichalcogenolate-Protected Copper and Silver Superatomic Nanoclusters and Their Alloys*. *Acc. Chem. Res*. **2018**, *51*, 2475-2483.
12. (a) Walter, M.; Akola, J.; Lopez-Acevedo, O.; Jadzinsky, P. D.; Calero, G.; Ackerson, C. J.; Whetten, R. L.; Gronbeck, H.; Hakkinen, H. A unified view of ligand-protected gold clusters as superatom complexes. *PNAS*, **2008**, *105*, 9157-9162. (b) Zhong, Y.-J.; Liao, J.-H.; Chiu, T.-H.; Kahlal, S.; Lin, C.-J.; Saillard J.-Y.; Liu, C. W. *A Two-Electron Silver Superatom Isolated from Thermally Induced Internal Redox Reaction of A Silver(I) Hydride. Angew. Chem. Int. Ed.* **2021**, *60*, DOI: 10.1002/anie.202100965.
13. Edwards, A. J.; Dhayal, R. S.; Liao, P. -K.; Liao, J. –H.; Chiang, M. –H.; Piltz, R. O.; Kahlal, S.; Saillard, J. –Y.; Liu, C. W. Chinese Puzzle Molecule: A 15 Hydride, 28 Copper Atom Nanoball. *Angew. Chem. Int. Ed*., **2014**, *53*, 7214-7218.
14. (a) Dhayal, R. S.; Liao, J.−H.; Lin, Y.−R.; Liao, P.−K.; Kahlal, S.; Saillard, J.-Y.; Liu, C. W. *A Nanospheric Polyhydrido Copper Cluster of Elongated Triangular Orthobicupola Array: Liberation of H_2 from Solar Energy*. *J. Am. Chem. Soc*. **2013**, *135*, 4704-4707. (b) Dhayal, R. S.; Liao, J. –H.; Wang, X.; Liu, Y. –C.; Chiang, M. –H.; Kahlal, S.; Saillard, J. –Y.; Liu, C. W. Diselonophosphate-Induced Conversion of an Achiral

[$Cu_{20}H_{11}\{S_2P(O^iPr)_2\}_9$] into a Chiral [$Cu_{20}H_{11}\{Se_2P(O^iPr)_2\}_9$] Polyhydrido Nanocluster. *Angew. Chem. Int. Ed*., **2015**, *54*, 13604-13608

15. Barik, S. B.; Huo, S. –H.; Wu, C. –Y.; Chiu, T. –H.; Liao, J. –H.; Wang, X.; Kahlal, S.; Saillard, J. –Y.; Liu, C. W. Polyhydrido Nanocluster with a Hollow Icosahedral Core: [$Cu_{30}H_{18}\{E_2P(OR)_2\}_{12}$] (E= S or Se; R= nPr, iPr, or iBu). *Chem. Eur. J*. **2020**, *26*, 10471-10479.
16. Lin, P. –Y.; Li, D. -Y.; Ho, F. –H.; Liao, J. –H.; Barik, S. K.; Liu, C. W. Unified reciprocity of dithiophosphate by dichalcogenophosph(in)ate ligands on copper hydride nanoclusters via ligand exchange reaction. *J. Chin. Chem. Soc*., **2019**, *66*, 987-994.
17. Chakrahari, K. K.; Liao, J.; Silalahi, R. P. B.; Chiu, T. –H.; Liao, J. –H.; Wang, X.; Kahlal, S.; Saillard, J. –Y.; Liu, C. W. Isolation and Structural Elucidation of 15-Nuclear Copper Dihydride Cluster: An Intermediate in the Formation of a Two-Electron Copper Superatom. *Small*. **2021**, 2002544.
18. Tang, Li.; Deng, S.; Wang, S.; Pei, Y.; Zhu, M. Total structural determination of alloyed $Au_{15.37}Cu_{16.63}$(S-Adm)$_{20}$ nanoclusters with double superatomic chains. *Chem. Commun*. **2021**, *57*, 2017-2020.
19. Steinfeld, J. I. Molecules and Radiation, an introduction, modern molecular spectroscopy; MIT Press: Cambridge, MA, 1981.
20. Tsai, C. N.; Mazumder, S.; Zhang, X. Z.; Schlegel, H. B.; Chen, Y. J.; Endicott, J. F. Are Very Small Emission Quantum Yields Characteristic of Pure Metal-to-Ligand Charge-Transfer Excited States of Ruthenium(II)-(Acceptor Ligand) Chromophores? *Inorg. Chem*. **2016**, *55*, 7341-7355.
21. Tsai, C. N.; Tian, Y.-H.; Shi, X.; Lord, R. L.; Schlegel, H. B.; Chen, Y. J.; Endicott, J. F. Experimental and DFT Characterization of Metal-to-Ligand Charge-Transfer Excited States of (Rutheniumammine)(Monodentate Aromatic Ligand) Chromophores. *Inorg. Chem*. **2013**, *52*, 9774-9790.
22. SAINT V4.043: Software for CCDC Detector System; Bruker Analystic X-ray Systems, Madison, WI, **1995**.
23. G. M. Sheldrick, SADABS, University of Göttingen, Göttingen, Germany, **1996**.
24. G. M. Sheldrick, Acta Crystallogr. **2008**, *A64*, 112.

25. SHELXL v6.14 (PC version) Program Library for Structure Solution and Molecular Graphics, Bruker Analytical X-ray Systems, Madison, WI, **1998**.

For Table of Content only:

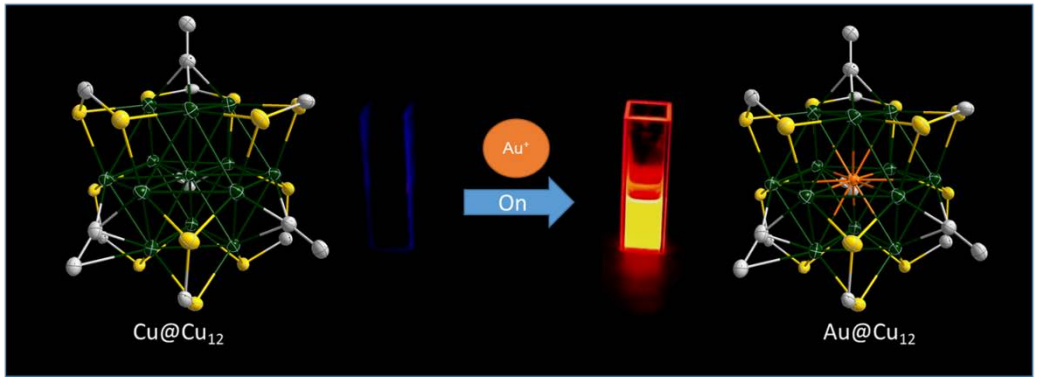

Compared to its homometallic $Cu@Cu_{12}$ counterpart, the presence of an Au atom in the center of the cubocathedral ($Au@Cu_{12}$) nanocluster significantly enhances its PL quantum yield to 55% at ambient temperature in solution.